Chapter 7 28 September 2004 M=6.0 Parkfield, California, earthquake

A M=6.0 earthquake along the Parkfield segment of the San Andreas fault struck Central California on 28 September 2004 at 17:15:26 UTC (10:15:26 am local time). The epicenter was located 11 km south-southeast of Parkfield, California, and 30 km northeast of Paso Robles, as reported by the Southern California Seismic Network. The mainshock nucleated at $35.815°N, 120.374°W$ at a depth of 7.9 km and ruptured towards the northwest. The rupture terminated about 3 km southeast of the San Andreas Fault Observatory at Depth (SAFOD), where a drilling for a deep borehole observatory intended to intersect the San Andreas began in June 2004. While the event was felt as far as San Francisco and Los Angles, there were no casualties and little reported damage. The preliminary magnitude estimate released by the USGS was M=5.8, which was later revised to M=6. This event is particularly interesting since there are numerous published hypotheses that might be included in the Bayes prior. These hypotheses are described briefly in the following Section.

7.1 Background: the Parkfield, California earthquake experiment

This earthquake generated much excitement in the seismological community because a predicted M=6 earthquake in the Parkfield segment of the San Andreas had been long overdue. Parkfield, of course, is the subject of a famous earthquake prediction experiment (Bakun and Lindh, 1985). It had been that observed moderately-sized earthquakes had occurred along the Parkfield section of the San Andreas at fairly regular intervals since the 1857 Fort Tejon earthquake - 1881, 1901, 1922, 1934, 1966.

The average interval between events is 22 years, and the next significant Parkfield event had been predicted to occur before 1993 (1966 + 22, with a 95% confidence interval of ±6 years) (Bakun and Lindh, 1985). While there was not much data available from the earlier events in the sequence, Bakun and McEvilly (1979) observed that the available seismograms from the 1922, 1934, and 1936 mainshocks were remarkably similar. In addition, the 1934 and 1966 sequences were both preceded by M=5 foreshocks about 17 minutes before the mainshock. The seismograms from the foreshocks were also remarkably similar. In both the 1934 and 1936 sequences, the foreshocks were located 1 to 2 km northwest of the mainshock epicenters and ruptured towards the northwest; both mainshocks ruptured towards the southeast. The aftershock patterns of the two sequences were also similar. These similarities suggested that characteristic earthquakes - earthquakes involving the same patch of fault failing in a time-predictable manner under the influence of uniform tectonic loading - were occurring at Parkfield. Characteristic earthquakes are at the heart of time-dependent probabilistic hazard models. They imply that earthquake hazard depends on time elapsed since the last event. While there were no available recorded ground motions prior to the 1922 event, Bakun and Lindh (1985) examined anecdotal reports on intensities and crack formation for the earlier events and concluded that they were similar to the 1934 and 1936 events. It was thus suggested that the next significant Parkfield event, expected to occur before 1993, would be similar to the previous sequences - a M=5 foreshock rupturing to the northwest would occur 17 minutes before the mainshock, the M=6 mainshock would rupture towards the southeast. The foreshock and mainshock were expected to nucleate in the Parkfield preparation zone, a 1-2 km stretch of fault near Middle Mountain, where there is a 5° degree change in strike of the fault trace and which includes the epicenters of the 1966 foreshock and mainshock. The mainshock was expected to rupture 20-25 km towards the southeast, terminating near Gold Hill, where there is a 1-km echelon offset of the fault trace (Bakun and Lindh, 1985).

In the time-predictable earthquake model, an earthquake occurs once it has recovered the stress released by the previous event (Stein, 2002). The predicted Parkfield

earthquake did not occur in 1988, nor within the 95% confidence interval (by 1993) of Bakun and Lindh (1985). In 2002, Murray and Segall (2002) showed that the stress released from the 1966 mainshock had been reaccumulated by 1987. They suggested possible explanations for the failure of the time-predictable model; these included the presence of fluids in the fault, complex interactions between various fault systems, dependence on past slip history not accounted for by the time-predictable model, and a possible change in strain rate in the 1990's. They suggest that perhaps a slip (rather than time) predictable model is more appropriate. In a slip-predictable model, the slip of the next earthquake would be equal to the slip accumulated since the previous event. In this case, the longer than average interval since the 1966 mainshock would predict that if the next Parkfield event happened in 2002, it would have to be M=6.6-6.9 - and the magnitude would grow larger the longer the wait.

How the M=6.0 2004 Parkfield earthquake changes beliefs regarding the idea of characteristic, time-predictable earthquake models is yet to be seen. It appears that the slip-predictable model over predicts the magnitude - from Murray and Segall, the 38 year interval since the 1966 event required the next event to be at least M=6.6-6.9. Can the 2004 event be considered a "characteristic" Parkfield event? There was no 17 minute foreshock, the epicenter did not occur in the Parkfield preparation zone, and the rupture propagated to the northwest as opposed to the expected southeast propagation. Does this mean the time-predictable model fails as well? On the other hand, if the 1936 event is included in the recurrence time calculation (but not including the 2004 event), the mean interval is still 21.8 years, but the standard deviation is closer to 7.2 years, as opposed to the standard deviation of 3.1 years from Bakun and Lindh (1985). (Bakun and Lindh did not include the 1934 sequence in calculating their standard deviation.) This puts the 95% confidence interval for the predicted date of the Parkfield event following the 1966 sequence at 1988 ± 14.4 years, placing the upper bound on the predicted date at 2002. The low precisions make for a very unimpressive prediction (and perhaps disqualify it as a prediction). However, it does imply that the 38 year interval between the 1966 and 2004 events is not as inconsistent with the time-predictable model as it has seemed.

Does the occurrence of the 2004 Parkfield event decrease the probability of a large earthquake on that portion of the San Andreas, as the slip-predictable model implies, or increase this probability by bringing other portions of the fault closer to failure through Coulomb stress transfer (Stein, 1999)? The data from the SAFOD project and continued monitoring of Parkfield and the high-density geodetic networks in Japan will hopefully shed more light on this problem.

7.2 Road map

Developing models of earthquake occurrence is an active area of research. It is not in the scope of this thesis to determine which models are appropriate for a given region - for instance, whether a time- or slip-predictable model is appropriate for Parkfield. However, such issues are potentially related to this thesis by means of the Bayesian prior. The Bayesian prior is meant to be a statement of our beliefs regarding where, when, and what size of earthquakes can occur. Ideally then, the prior would include models of earthquake occurrence. When, in the future, there are *well-accepted and validated* models of earthquake occurrence that take into account and accurately quantify (with fairly good precision) the effects of factors such as stress transfer, repeatability of earthquakes, role of fluids in fault zones, dynamic and tidal triggering, then can be used to define the prior. The Parkfield predictions will not be included in the Bayes prior in this example, tempting though it might be with the abundance of strong opinions about Parkfield. Instead, same types of prior information used in the preceding examples - station geometry, previously observed seismicity, and the Gutenberg-Richter relationship- will be applied. Similar to the San Simeon example, the San Andreas fault trace will be included in the Bayes prior, since it is such a prominent feature and no one would disagree that the San Andreas is a likely location for earthquakes. Again, the use of available arrivals and constraints from not-yet-arrived data are technically observations. However, they are considered with the prior (and not the likelihood) since they do not involve observed amplitudes.

Following a brief discussion of station geometries in the epicentral region, the VS

single station estimates for magnitude and epicentral distance based on the initial 3 seconds of data are presented. The effect of different types of prior information (in particular, the Gutenberg-Richter relationship) are evaluated. Updated VS estimates at 6, 12, 27, and 77 seconds after the initial P detection are presented. Amplitude-based locations, and how the peak observed amplitudes compare with the envelope attenuation relationships are also discussed.

7.3 SCSN stations in the epicentral region

Figure 7.1 shows the operating BDSN and SCSN stations within 250 km of the epicenter of the 2004 M=6.0 Parkfield mainshock. The polygons define the nearest neighbor regions of the stations about which they are centered. If station A has the first P-wave detection from an event, the earthquake is constrained to be within station A's Voronoi cell. The first triggered station is PKD (Parkfield), located about 20 km away from the epicenter of the mainshock. PKD's Voronoi cell is shaded in Figure 7.1. The Voronoi cells near the epicenter are relatively large. The density of digital stations with real-time telemetry in this region is relatively low, compared to other regions in California (for example, the Los Angeles basin to the southeast). Table 7.1 lists the locations, Voronoi areas, epicentral distance, fault distance, and P wave arrival times at stations sharing Voronoi edges with PKD. The Voronoi areas around Parkfield are about two orders or magnitude larger than those in surrounding the Yorba Linda mainshock (Chapter 8). Stations at Park Hill (PHL) and the San Andreas Geophysical Observatory (SAO) have Voronoi areas on the order of 40,000 km^2. Voronoi areas on this order will be characteristic of stations located on the outer boundaries of the network. The locations of earthquakes $M \geq 1$ reported by the network in the 24 hours preceding the mainshock are marked by circles. Most of the seismicity before the Parkfield mainshock was concentrated in the Mammoth Lakes region. There was an M=1.78 event a few kilometers off the San Andreas, 26 km northwest of station PKD within PKD's Voronoi cell. This event is most likely in the aftershock sequence of an M=3.71 event (located by the Berkeley Digital Seismic

Network) which occurred on 26 September, and is probably not a foreshock to the M=6 mainshock.

Figure 7.2 shows the observed vertical acceleration records from PKD and the stations sharing a Voronoi edge with PKD. The second P arrival is at station PHL, approximately 4.4 seconds after the initial P detection at PKD. The vertical lines marked "T0" and "T1" are the theoretical P and S wave travel times given the reported location for the epicenter of $35.82°N, 120.37°W$.

Stations closest to the 2004 $M = 6.0$ Parkfield mainshock

Station name	Abrev	Lon	Lat	vor. area km^2	ep. dist. km	fault dist. km	P-Arrv. sec
Parkfield	PKD	-120.54	35.945	13,371	20.81	1.73	3.03
Park Hill	PHL	-120.55	35.408	39,775	48.43	45.4	7.47
Simmler	SMM	-119.996	35.314	4,610	65.57	59.7	10.19
Rector	RCT	-119.24	36.305	11,887	114.9	111.4	17.95
Vestal	VES	-119.08	35.841	3,757	116.16	112.05	18.15
SanAndr.Obs.	SAO	-121.45	36.764	39,930	142.61	112.3	22.25

Table 7.1: Some stations within 150 km of the 2004 M=6.0 Parkfield mainshock. The station closest to the epicenter is Parkfield (PKD), at an epicentral distance of 21 km. The other stations listed share a Voronoi edge with PKD. Stations PHL and SAO have very large Voronoi areas because they are along the edge of the seismic network. The Voronoi areas of stations along the boundaries of the network are about two orders of magnitude larger than those in its most densely instrumented regions. (Compare with Table 8.1 in Chapter 8 for stations in the proximity of the Yorba Linda mainshock.)

7.4 Single station estimates: solving for magnitude and epicentral distance

With data from only a single station, the VS method can be used to solve for magnitude and epicentral distance, or magnitude and location coordinates. The VS estimates for magnitude and epicentral distance using the first 3 seconds of data from PKD are presented first.

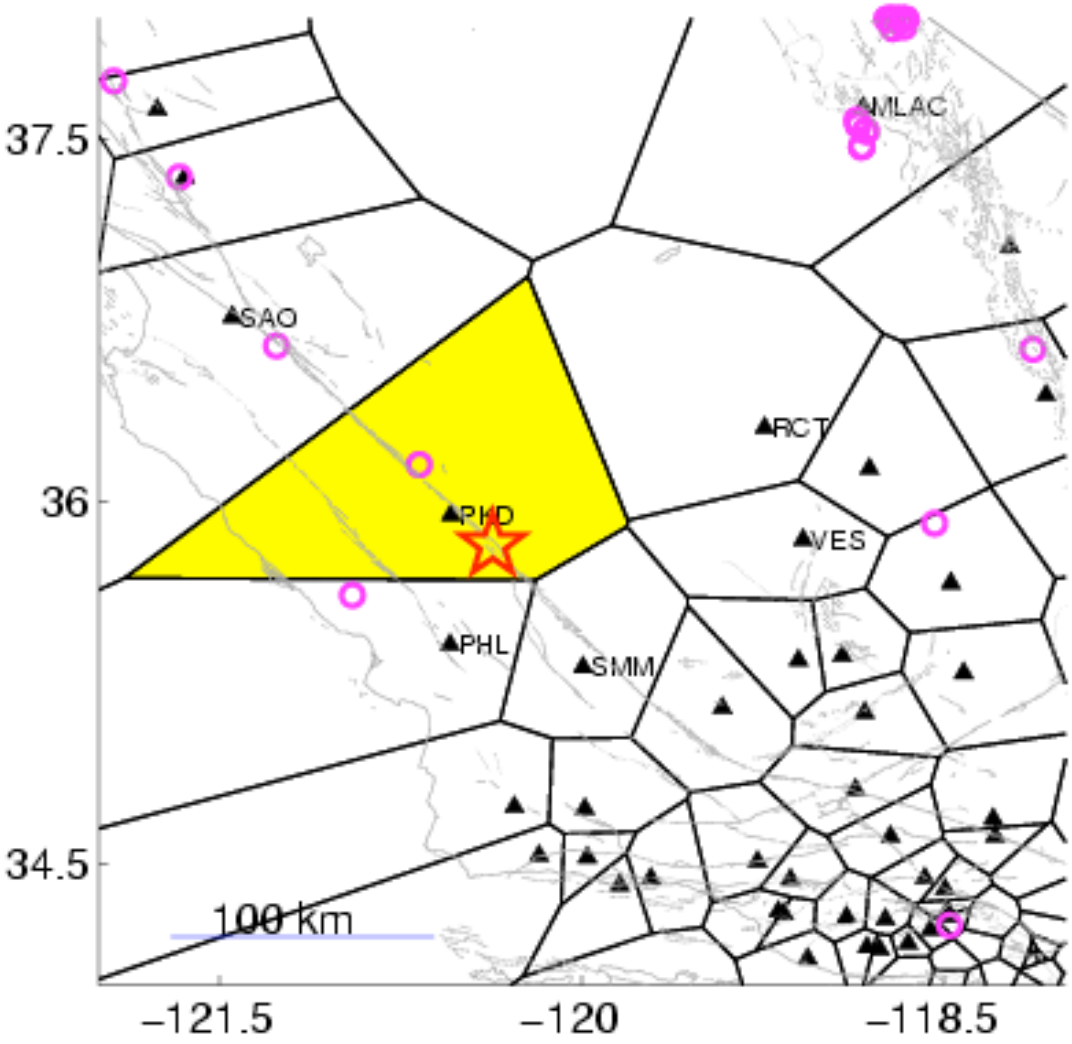

Figure 7.1: Map of BDSN and SCSN stations that recorded ground motions from the 28 September 2004 $M = 6.0$ Parkfield, California earthquake. Circles are locations of $M \geq 1$ earthquakes which occured in the 24 hours prior to the mainshock. There were 71 $M \geq 1$ events in the region bounded by longitudes $124°W$ and $116°W$, and latitudes $32°N$ and $40°N$. Most of these were concentrated in the Mammoth Lakes region. One such event was located in the Voronoi cell of PKD, the closest station to the epicenter.

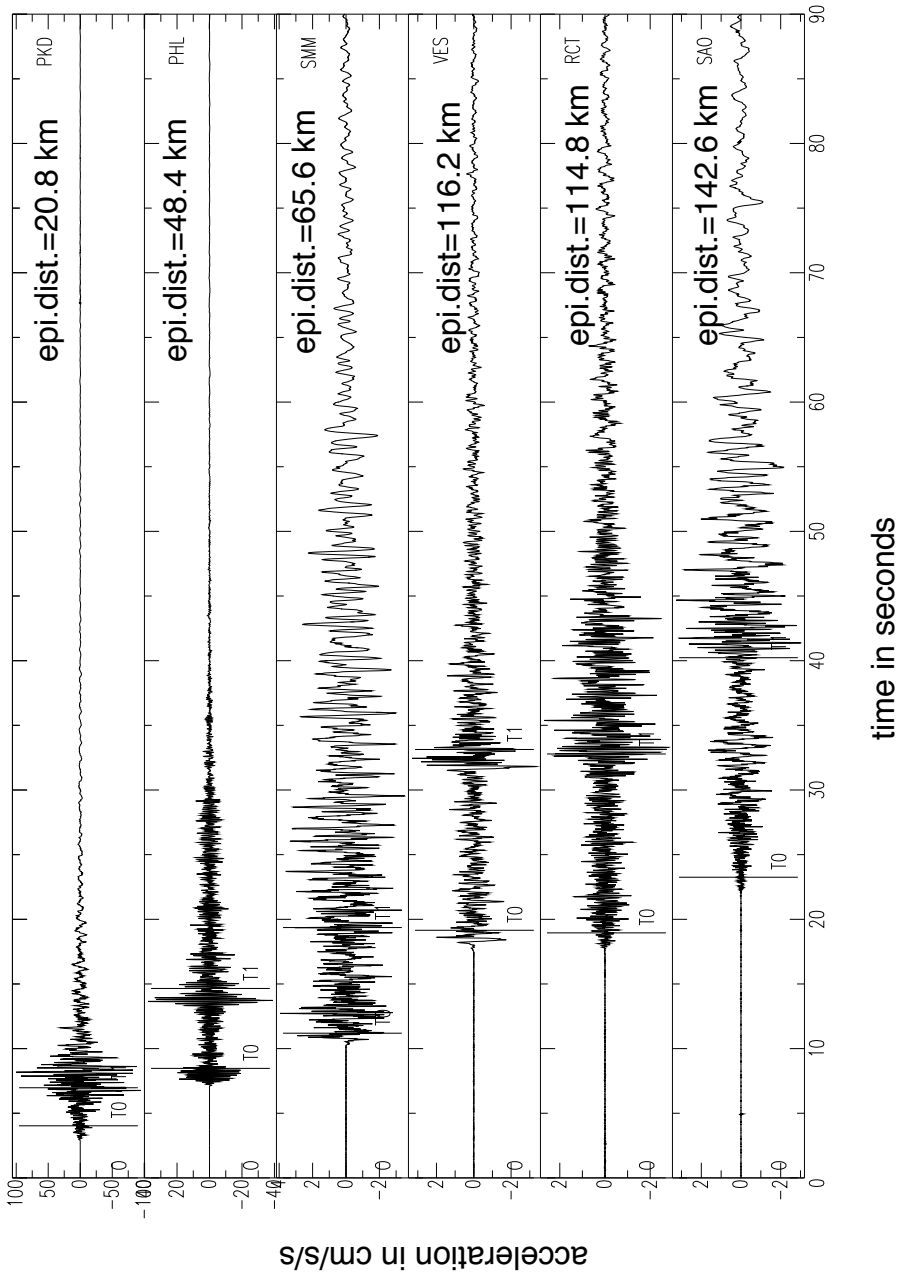

Figure 7.2: Vertical acceleration records from stations within 150 km of the 2004 M=6.0 Parkfield mainshock epicenter. Vertical lines marked "T0" and "T1" are the predicted P and S arrival times using Eaton's travel time code, a 6 layer, 1 D Southern California velocity model, and the SCSN-reported location of $35.82°N, -120.37°W$.

Let Z.a, Z.v, and Z.d refer to the maximum vertical acceleration, velocity, and filtered displacement envelope amplitudes observed between the P detection at a station and some time t. (In the examples in this thesis, it is assumed that P-waves can be detected efficiently using short-term over long-term average methods.) EN.a, EN.v, and EN.d are the corresponding envelope amplitudes for the root mean square of the maximum amplitudes of the horizontal channels.

Figure 7.3(a) shows the P/S discriminant function (discussed in Appendix C) as a function of time. Recall that the P/S discriminant function is $PS = 0.4\log_{10}(Z.a) + 0.55\log_{10}(Z.v) - 0.46\log_{10}(EN.a) - 0.55\log_{10}(EN.v)$. The first zero crossing of P/S after the P arrival indicates the S-wave arrival. Figure 7.3(b) shows the ground motion ratio $Z_{ad} = Z.a^{0.36}/Z.d^{0.93} = 0.36\log_{10}(Z.a) - 0.93\log_{10}(Z.d)$ as a function of time. The left-hand axis shows the P-wave decision boundaries; those on the right, the S-wave decision boundaries. The ground motion ratio, Z_{ad}, from the first 3 seconds of data at PKD indicate that the event is in the group $M \geq 6$.

The likelihood function described in Chapter 4 (Eqn. 4.62) combines the magnitude estimates from the vertical acceleration and displacement ground motion ratio, along with the peak available vertical velocity, and rms horizontal acceleration, velocity, and displacement amplitudes to estimate magnitude and epicentral distance. Maximizing the likelihood function yields the source estimates (in this case, magnitude M and epicentral distance R_{PKD}) that are most consistent with the available observations. Figure 7.4 shows contours of the likelihood function expressed in terms of M and R. The likelihood is scaled to have a maximum value of 1; contours are drawn at the 0.6, 0.1, and 0.01 levels, which correspond to $\pm 1\sigma$, $\pm 2\sigma$, and $\pm 3\sigma$ for a 1-d Gaussian pdf. The "high" probability region within the 0.6 level contour is shaded; the actual magnitude and epicentral distance (star) is included in this region. Trade-offs between M and R cannot be resolved by the 3 second observations; this is evident from the elongated contours of the likelihood function. In the absence of additional data, such trade-offs can be resolved by introducing prior information into the estimation process. While trade-offs do exist, the likelihood function does have a peak. An M=6.9 event located 50 km away from PKD is the source estimate

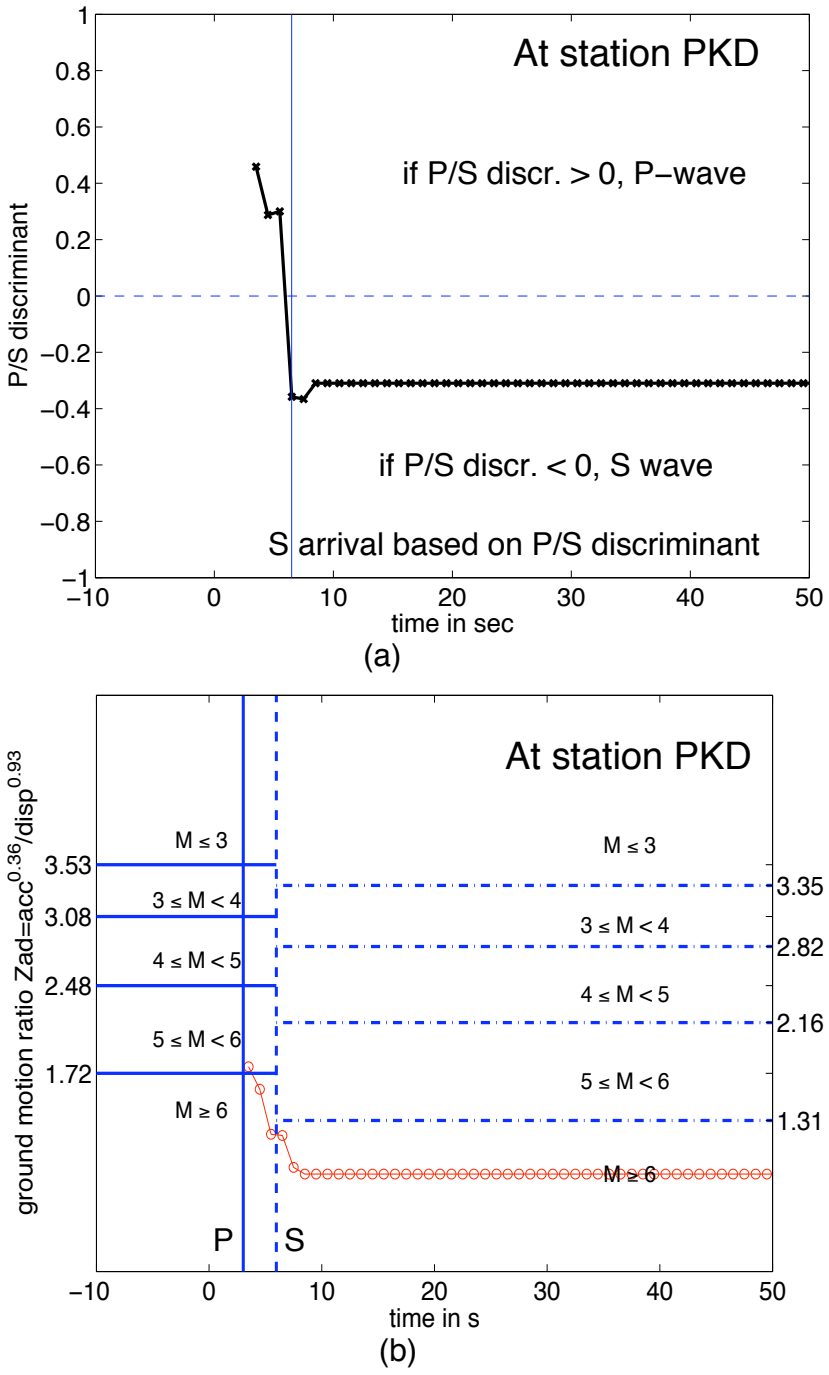

Figure 7.3: (a) The P/S discriminant $PS = 0.43\log_{10}(Z.a_{max}) + 0.55\log_{10}(Z.v_{max}) - 0.46\log_{10}(EN.a_{max}) - 0.55\log_{10}(EN.v_{max})$ at PKD as a function of time. The first zero crossing of PS after the P-wave arrival indicates the S-wave arrival. The P/S discriminant puts the S-wave arrival between $t = 5.5, 6.5$ seconds; the predicted S-wave arrival given the SCSN-reported location is $t = 5.75$ seconds. (b) The ground motion ratio $Z_{ad} = \frac{acc^{0.36}}{disp^{0.93}}$ at PKD as a function of time. The decision boundaries on the left are for P-wave amplitudes; those on the right for S-wave amplitudes. The ground motion ratios consistently indicate that the event is $M \geq 6$.

most consistent with the 3 second observed amplitudes. The Parkfield mainshock had M=6.0 and an epicenter 21 km away from PKD. When expressing the problem

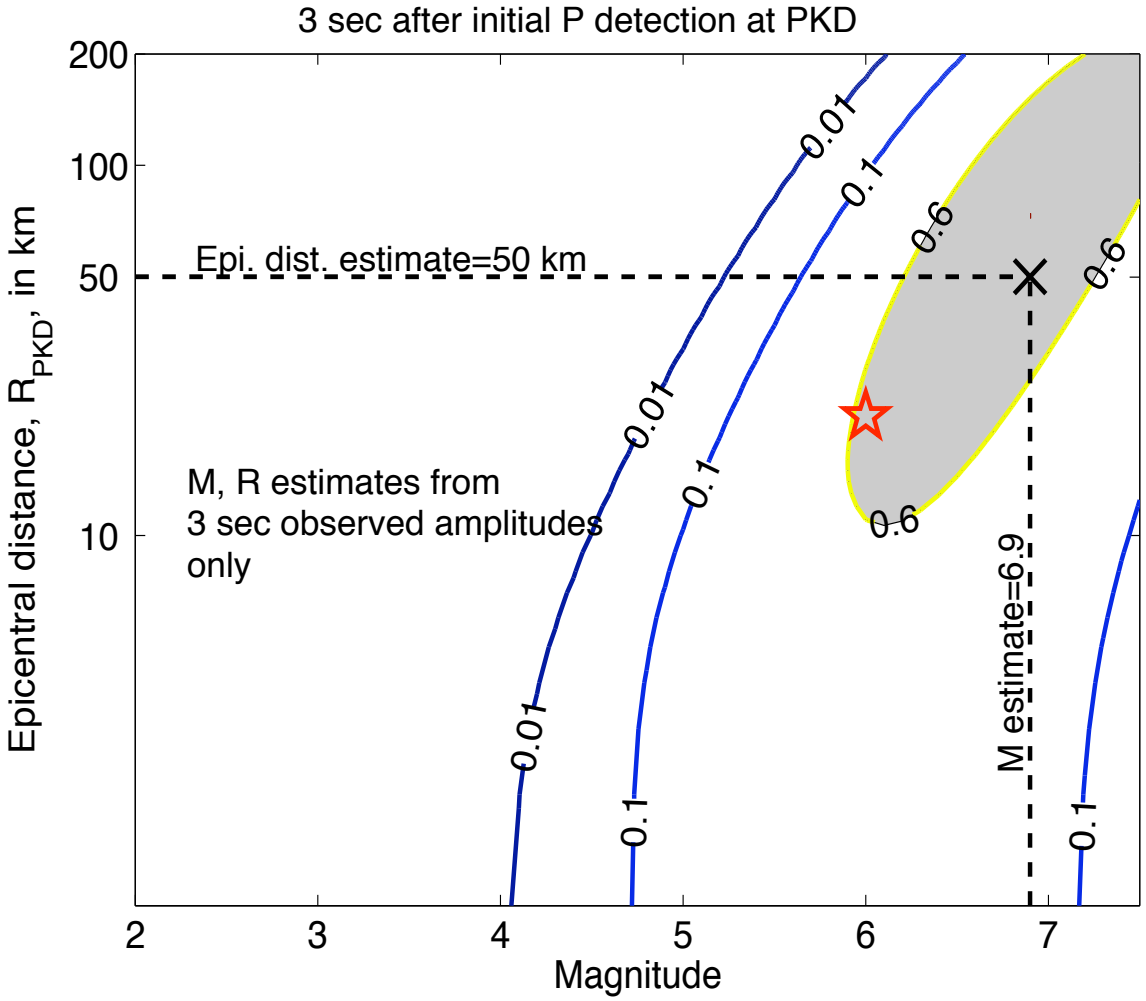

Figure 7.4: Contours of the likelihood function (expressed in terms of magnitude and epicentral distance) given the amplitudes at PKD 3 seconds after the initial P detection. Contours are drawn at 0.6, 0.1, 0.01 levels. Regions where the likelihood function has value > 0.6 are shaded. A star marks the actual magnitude and epicentral distance from PKD. An x marks the peak of the likelihood function.

in terms of magnitude and epicentral distance, the only prior information that can be included are 1) the range of epicentral distances consistent with the Voronoi cell of the first triggered station and 2) the Gutenberg-Richter magnitude-frequency relationship. If all locations within PKD's Voronoi cell are given equal weight, certain

epicentral distances will be more likely. A probability density function for epicentral distances consistent with being within PKD's Voronoi cell can be constructed. The lack of P arrivals at adjacent stations $\Delta t = 3$ seconds after the initial P detection provides further constraints on possible locations (and hence epicentral distances) (Figure 7.5). In Figure 7.6(b), the solid line (black) shows the pdf of possible epicentral distances (scaled to a maximum value of 1) consistent with a first arrival at station PKD, the dashed line shows the pdf of possible epicentral distances accounting for the non-arrivals at the adjacent stations $\Delta t = 3$ seconds after the initial P detection at PKD.

The VS estimates at any given time are the most probable source estimates given the available data (amplitudes) and the prior information (including arrivals and non-arrivals). They maximize the Bayesian posterior pdf, as discussed in Chapter 4. At 3 seconds after the initial P detection, the set of observations is still very sparse and the prior has much weight. The contours of the posterior pdf (whose "high" probability regions correspond to the VS estimates) with different priors are shown in Figure 7.7. From comparing (a) and (b) in Figure 7.7, whether or not the non-arrival information is included has not much effect. It is necessary to use the Gutenberg-Richter (G-R) relationship to get the "high" probability region of the Bayes posterior to include the actual magnitude and epicentral distance (star).

7.5 Multiple station estimates: solving for magnitude and epicentral location

The VS estimates for magnitude, latitude, and longitude at 6, 9, 15, 30, and 80 seconds after the earthquake origin time (or 3, 6, 12, 27, and 77 seconds after the initial P detection) will be discussed. Figure 7.8 shows to which stations (triangles) the P waves will have propagated to at the times of the updates. At each of the update times (labeled in seconds after the origin time on the contours), only stations with at least 3 seconds of data from the P wave arrival at that station will be included.

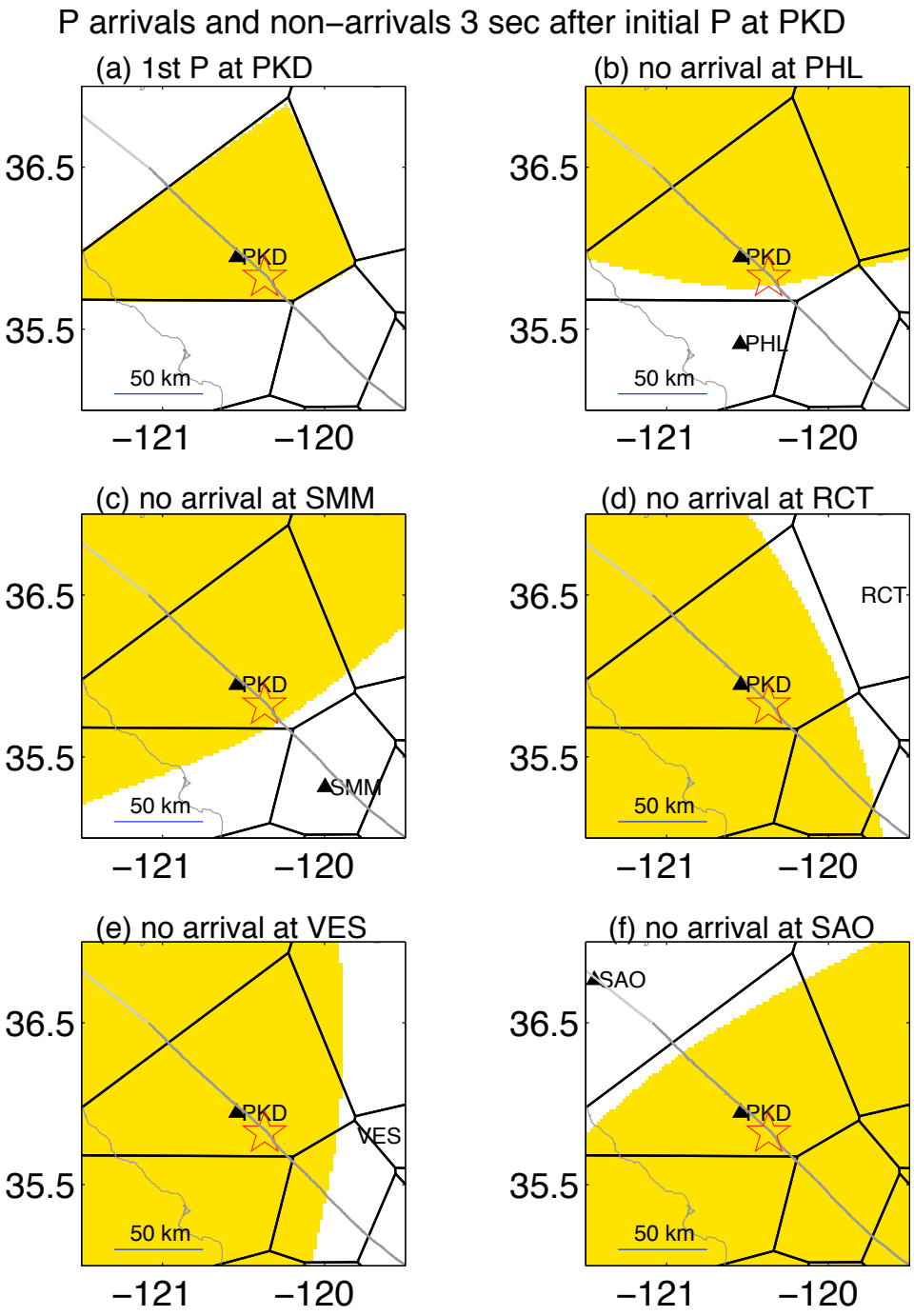

Figure 7.5: The shaded regions are those consistent with (a) the first P detection at PKD, and (b-f) no arrivals at PHL, SMM, RCT, VES, and SAO (they share a Voronoi edge with PKD) at the time of the first VS estimate 3 seconds after the initial P detection.

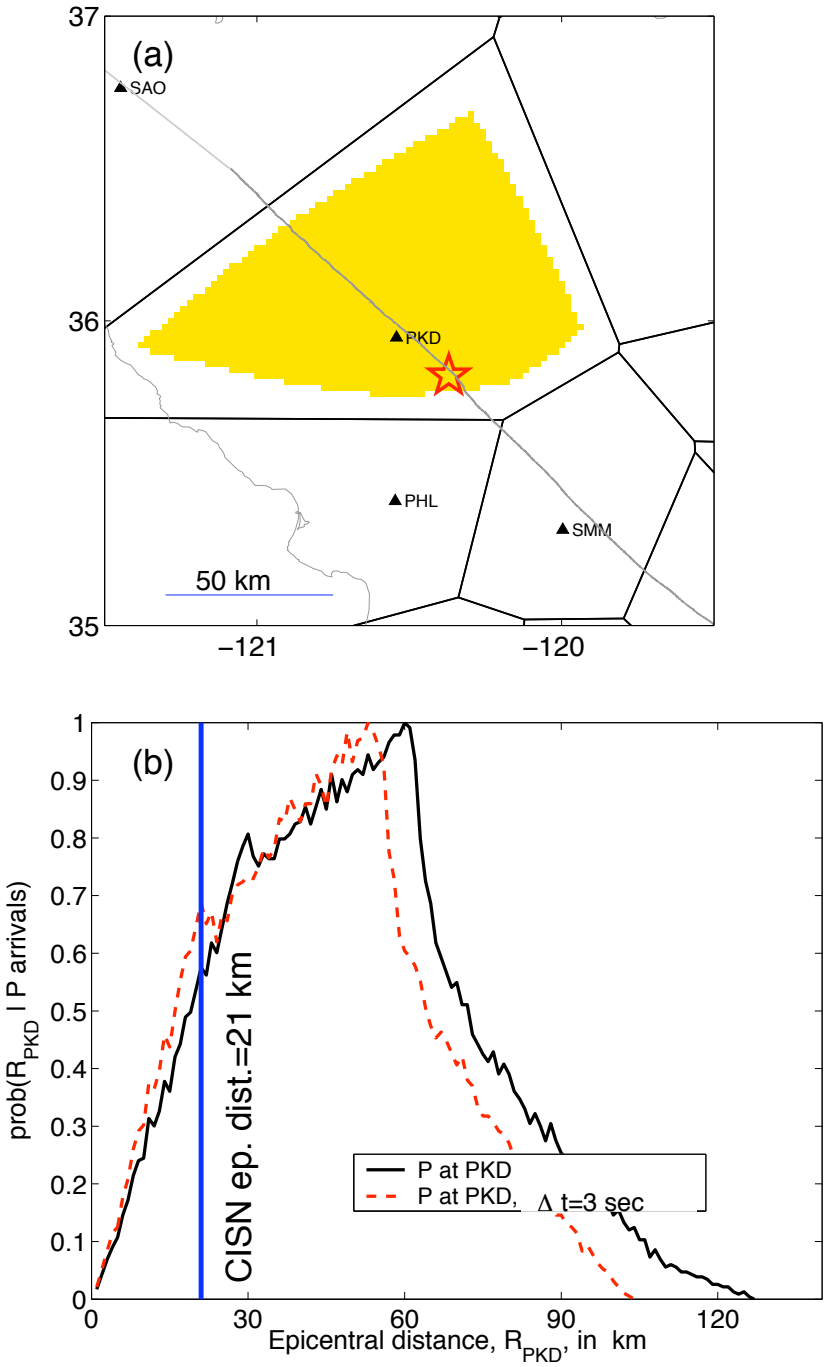

Figure 7.6: (a) The region of possible location is shaded. It is constrained by P-wave arrival at PKD and non-arrivals adjacent stations PHL, SMM, RCT, VES, and SAO $\Delta t = 3$ seconds after the initial P detection. (b) The range of possible epicentral distances, R_{PKD} with 1) the first P arrival at PKD (solid line), and 2) taking into account that there are no other subsequent arrivals 3 seconds after the initial P detection. The vertical line shows the epicentral distance using the SCSN-reported location.

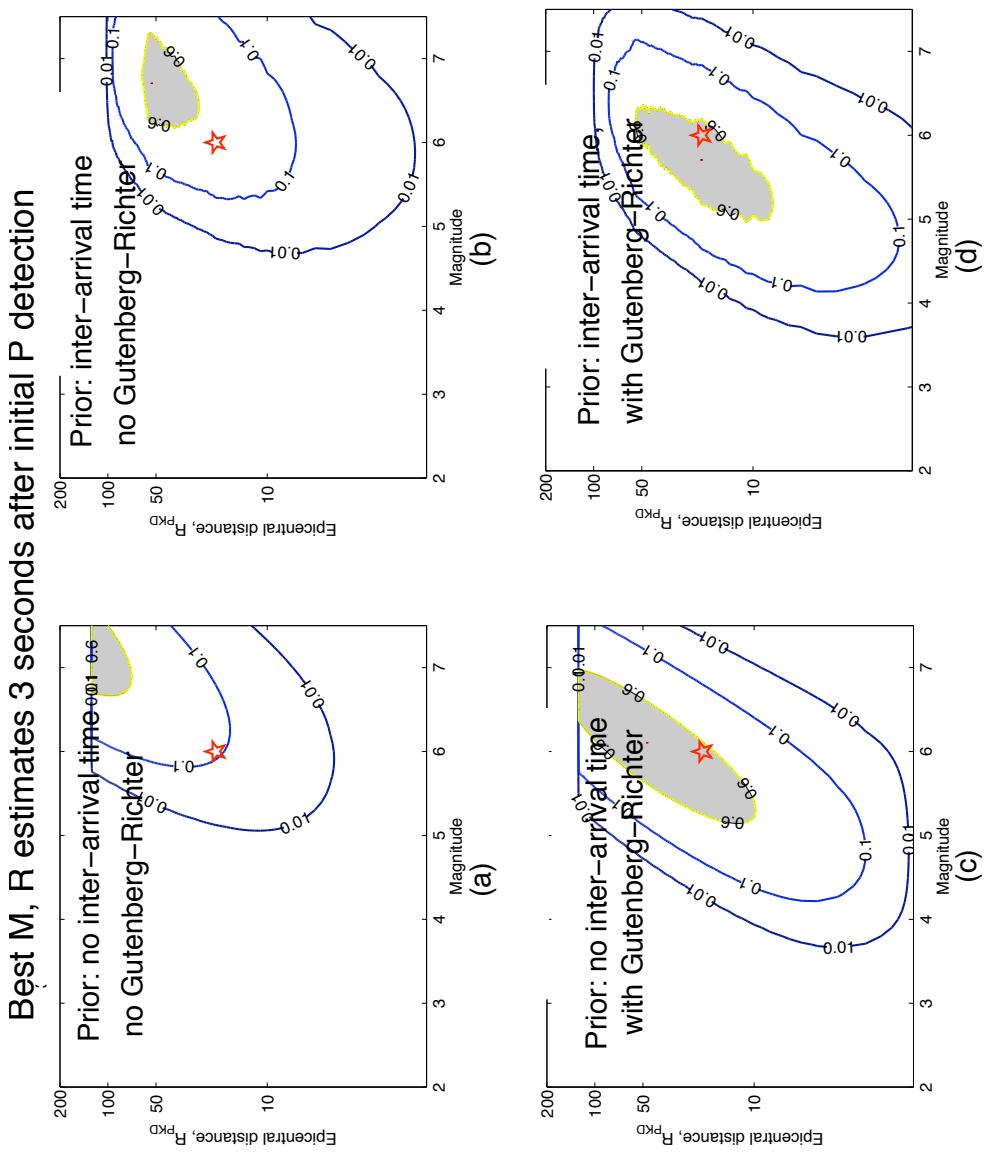

Figure 7.7: The effects of different types of prior information on the Bayesian posterior pdf, $prob(M, R|data)$ 3 seconds after the initial P detection at PKD. The differences are due to the different types of prior information used. Comparing (a) and (b) shows the effect of taking into account that there are no other arrivals 3 seconds after the initial P detection. Comparing (a) and (c) (or (b) and (d)) shows the effect of using the Gutenberg-Richter magnitude-frequency relationship.

The 80 second contour is beyond the boundaries of the plot. It includes all the 49 stations shown. The hashed line shows the extent of the rupture from a preliminary slip inversion by Chen Ji available on the CISN/SCSN website (http://www.cisn.org,).

Given only the peak amplitudes at PKD 3 seconds after the initial P detection (no prior information), Figure 7.9 shows the locations consistent with 6 different magnitude ranges: $2 \leq M < 3$, $3 \leq M < 4$, $4 \leq M < 5$, $5 \leq M < 6$, $6 \leq M < 7$, and $M \geq 7$. For each magnitude range, the contours of the location marginal of the likelihood function (integrated over the given magnitude range and scaled to a maximum value of 1) are drawn at the 0.01, 0.1, and 0.6 levels. The regions where $prob(lat, lon|data) \geq 0.6$ are shaded. In general, the area consistent with larger magnitudes is much larger than the regions consistent with smaller magnitudes.

Using a geographic coordinate system allows for the inclusion of previously observed seismicity and fault locations into the prior. The seismicity prior is generated by assigning locations within a 5 km radius of an earthquake in the previous 24 hours a weight of 10; all other locations have a weight of 1. The San Andreas fault prior is generated by assigning locations within 2 km of the San Andreas a weight of 10; all others have a weight of 1. The station geometry prior is generated by assigning locations within the translated edges of the first triggered station's Voronoi cell a weight of 100; all other locations have a weight of 1. These are then scaled such that they integrate to 1 over the range of possible latitude and longitudes. The location prior $prob(lat, lon)$ (Figure 7.10) is then obtained by multiplying the seismicity, San Andreas, and station geometry priors. The VS updates are calculated with and without the Gutenberg-Richter relationship. When the Gutenberg-Richter is used, the magnitude prior has the form $prob(M) = 10^{1-M}$, when it is not, the magnitude prior is $prob(M) = k$, where k is constant. Again, the magnitude prior is scaled so that it integrates to 1 over the magnitude range considered ($2 \leq M \leq 7.5$). The Bayesian prior is the product of the magnitude and location priors. That is, $prob(M, lat, lon) = prob(M) \times prob(lat, lon)$. $prob(lat, lon)$ is peaked at the location of the M=1.78 event near the San Andreas. In practice, foreshock/aftershock statis-

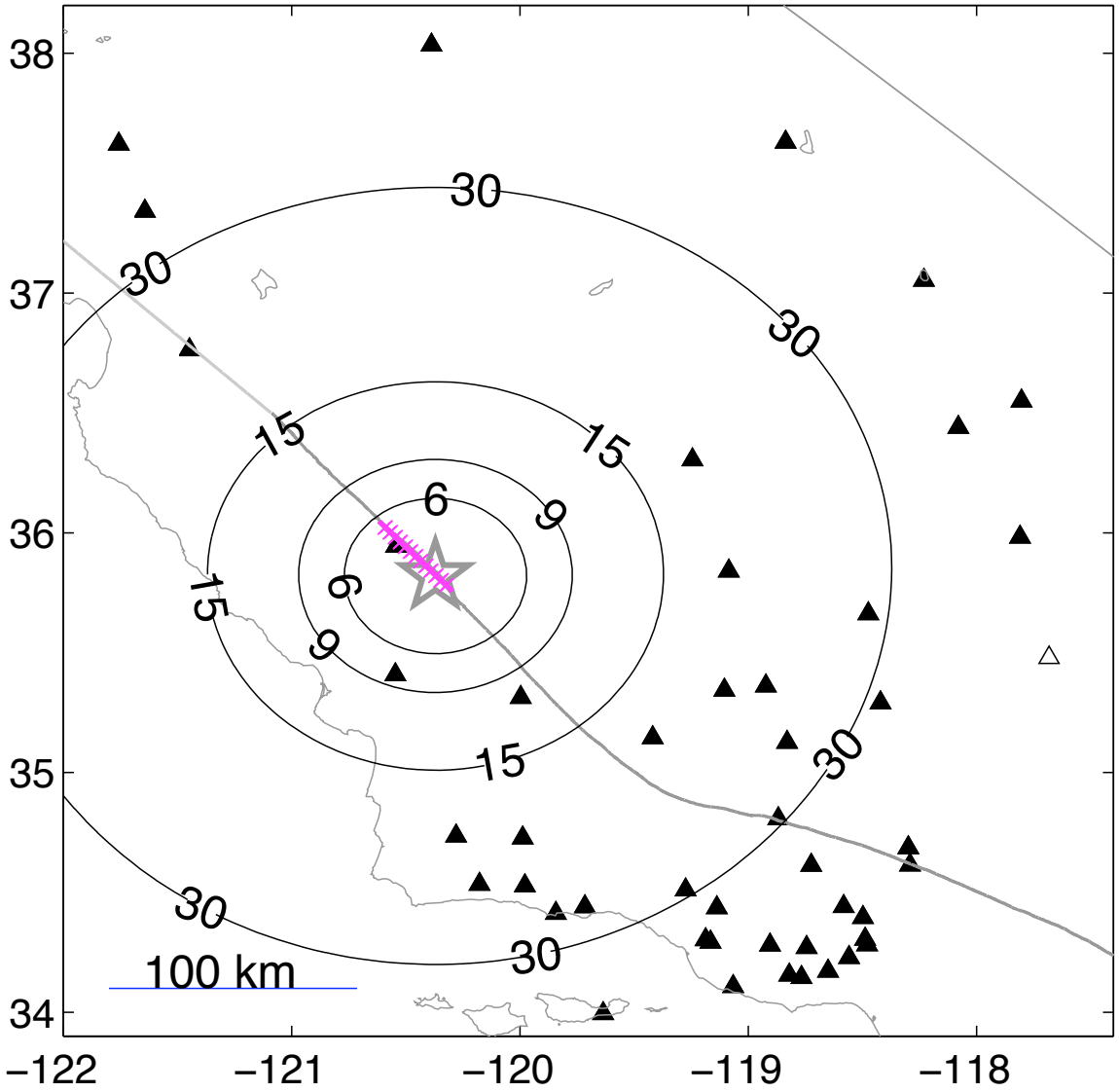

Figure 7.8: BDSN and SCSN stations operating at the time of the 2004 M=6.0 Parkfield, California mainshock. Contours show the P-wave wavefront (for a point source at the epicenter) at the times for which the VS estimates are updated. The contours are labeled with VS estimate times relative to the origin time - subtract 3 seconds to get time relative to initial P detection. The 80 second contour is beyond the boundaries of the plot.

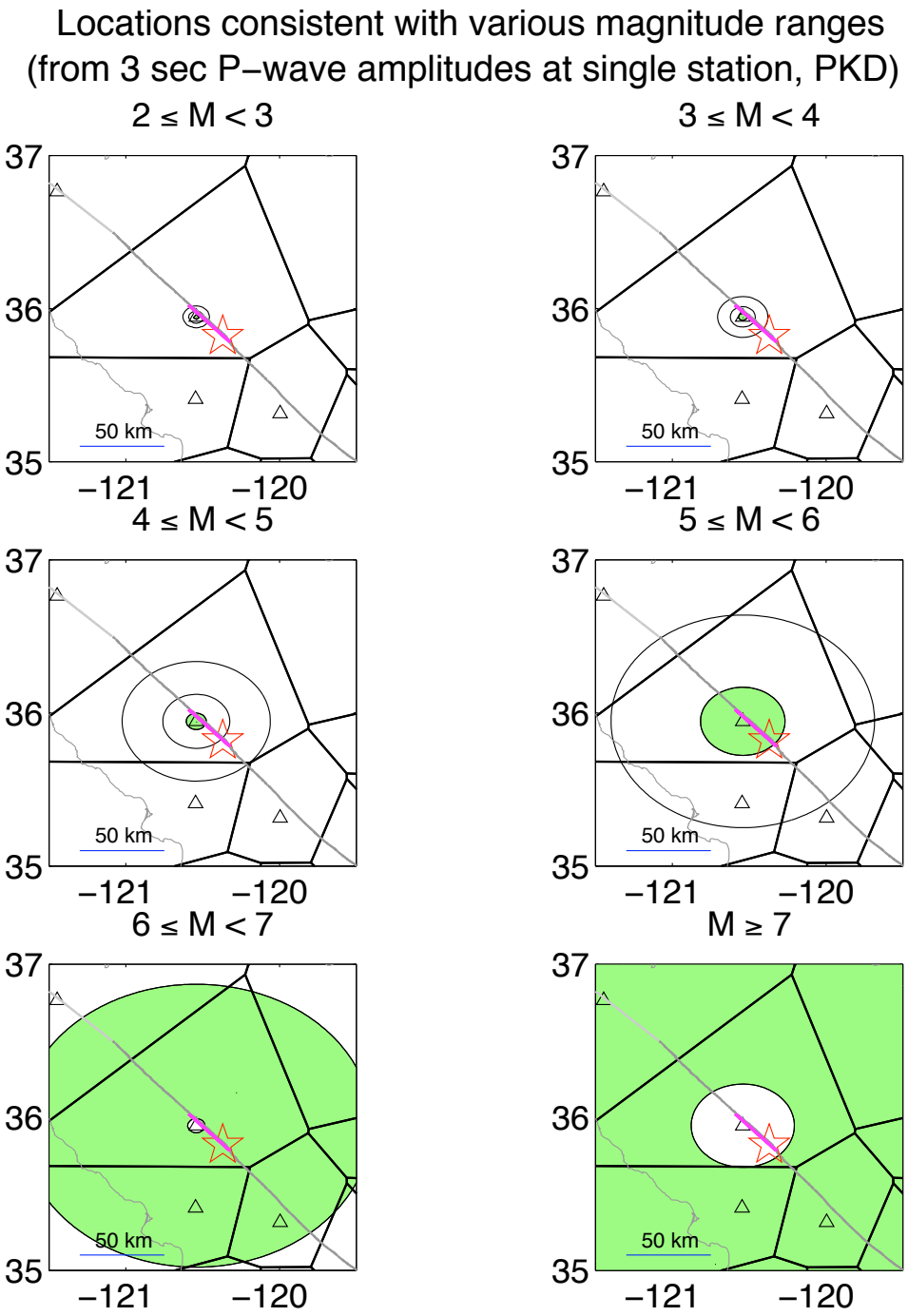

Figure 7.9: The shaded regions in each subplot are the locations consistent with the indicated magnitude range using the peak P-wave amplitudes 3 seconds after the initial P detection at PKD (no prior information included). The total area of the shaded "high probability" regions is much larger for events with $M \geq 5$ than for smaller magnitudes. 3 seconds of P-wave amplitudes from the first triggered station cannot uniquely resolve magnitude and location (although this information is enough to broadly estimate the probable magnitude range). The trade-offs shown here are comparable to those shown in Figure 7.4.

tics (Reasenberg and Jones, 1989) or short-term earthquake forecasts (Gerstenberger et al., 2003) should be used to generate the seismicity and fault location priors.

At 3 seconds after the initial P detection, VS location estimate (marked by an arrow on Figure 7.11) is the intersection of the 2 km band either side of the San Andreas and the 5 km radius about the M=1.78 event the previous day within PKD's Voronoi cell. The VS magnitude estimate without the G-R is $M = 6.5 \pm 0.65$; with the G-R, it is $M = 5.5 \pm 0.72$. At 6 seconds after the initial P detection, the P waves have propagated to the second closest station, PHL. The time between the first and second P arrivals is approximately 4.4 seconds. The second arrival constrains the location to lie along the hyperbola defined by $R_{PHL} - R_{PKD} = V \times 4$, where V is an average P-wave velocity.

By 12 seconds after the initial P detection at PKD, the P-waves arrive at a third station, SMM. With 3 arrivals, there is a uniquely determined epicenter. However, the magnitude estimates continue to evolve. Figure 7.13 shows the availability of P- and S-wave amplitudes as a function of VS estimate time. Figure 7.14 shows the evolution of the magnitude estimates. The magnitudes from maximizing the likelihood function (without the prior) are labeled "amplitudes only". Those labeled "VS" have station geometry, not-yet-arrived data, previous seismicity, and the San Andreas fault location in the Bayes prior. VS estimates with and without the Gutenberg-Richter relationship are shown. The uncertainties are initially large, but decrease like like $\frac{1}{\sqrt{N}}$, where N is the number of stations contributing data. Figure 7.15 shows the evolution of the VS location estimates as a function of time.

While they may not be as useful for seismic early warning, the latter VS estimates (using no prior information) provide amplitude-based location estimates that can be used as a check on the arrival-based locations that are generated by the seismic network. In general, minimizing the residuals between the predicted and observed arrival times is the most precise way to locate earthquake. However, timing-based locations can be prone to large errors, for instance, when two separate earthquakes are propagating ground motions to the stations concurrently. Location estimates based on the distribution of observed ground motion amplitudes are not precise, but

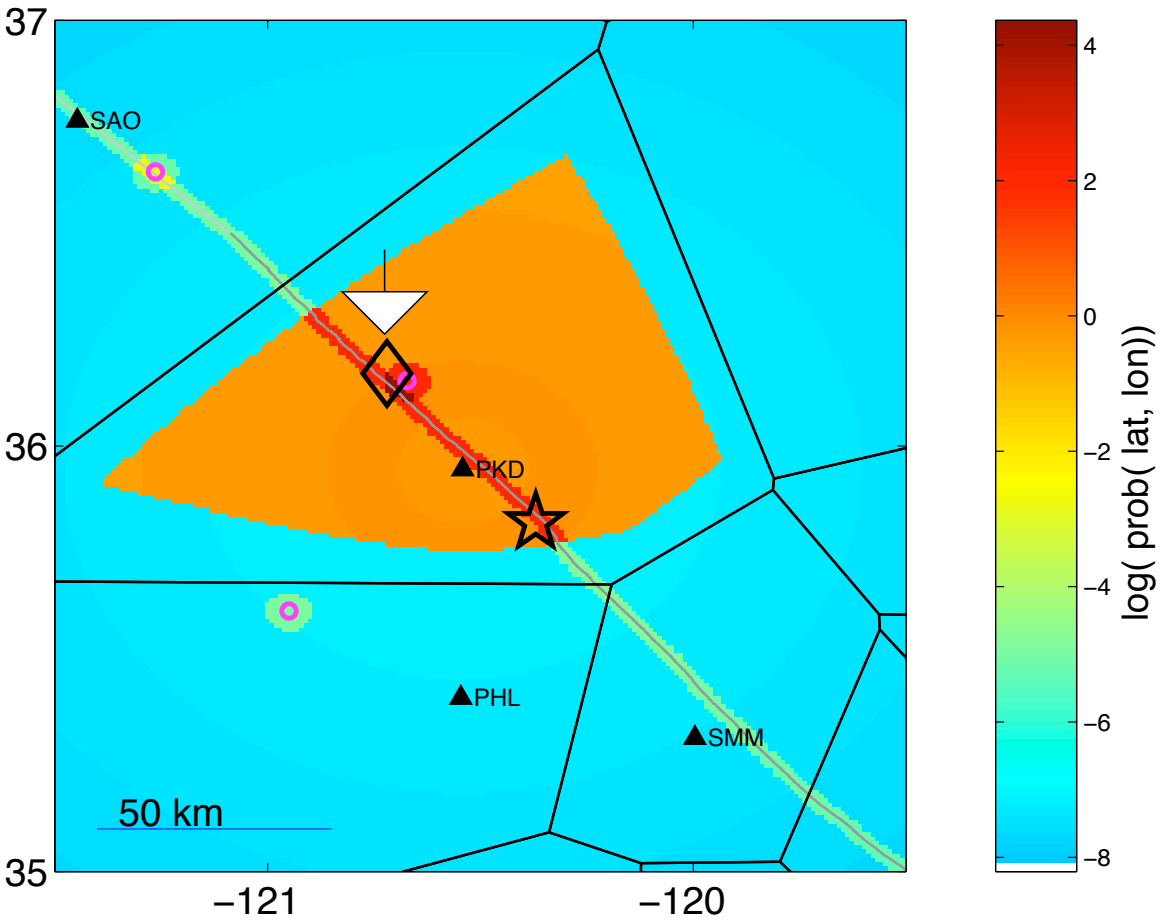

Figure 7.10: The (log of the) Bayesian prior pdf, $prob(lat, lon)$. The types of information included are: station geometry, arrival at PKD and non-arrivals at surrounding stations, previous seismicity (circles), and fault location. The region of possible location, as constrained by the first arrival at PKD and the non-arrivals at surrounding stations $\Delta t = 3$ seconds later is the convex region within PKD's Voronoi cell. Within this region of possible location, areas within a 2 km band of the San Andreas are given high probability. The peak of the prior pdf to the northwest of PKD (denoted by the white arrow) is due to an event in the preceding 24 hours located close to the San Andreas. This previous earthquake (M=1.78) is probably not related to the Parkfield mainshock. There had been a M3 event in that vicinity in the week preceding the mainshock; this M1.78 event was most likely part of the aftershock sequence of the M3. The event in PHL's Voronoi cell is probably an aftershock of the San Simeon earthquake.

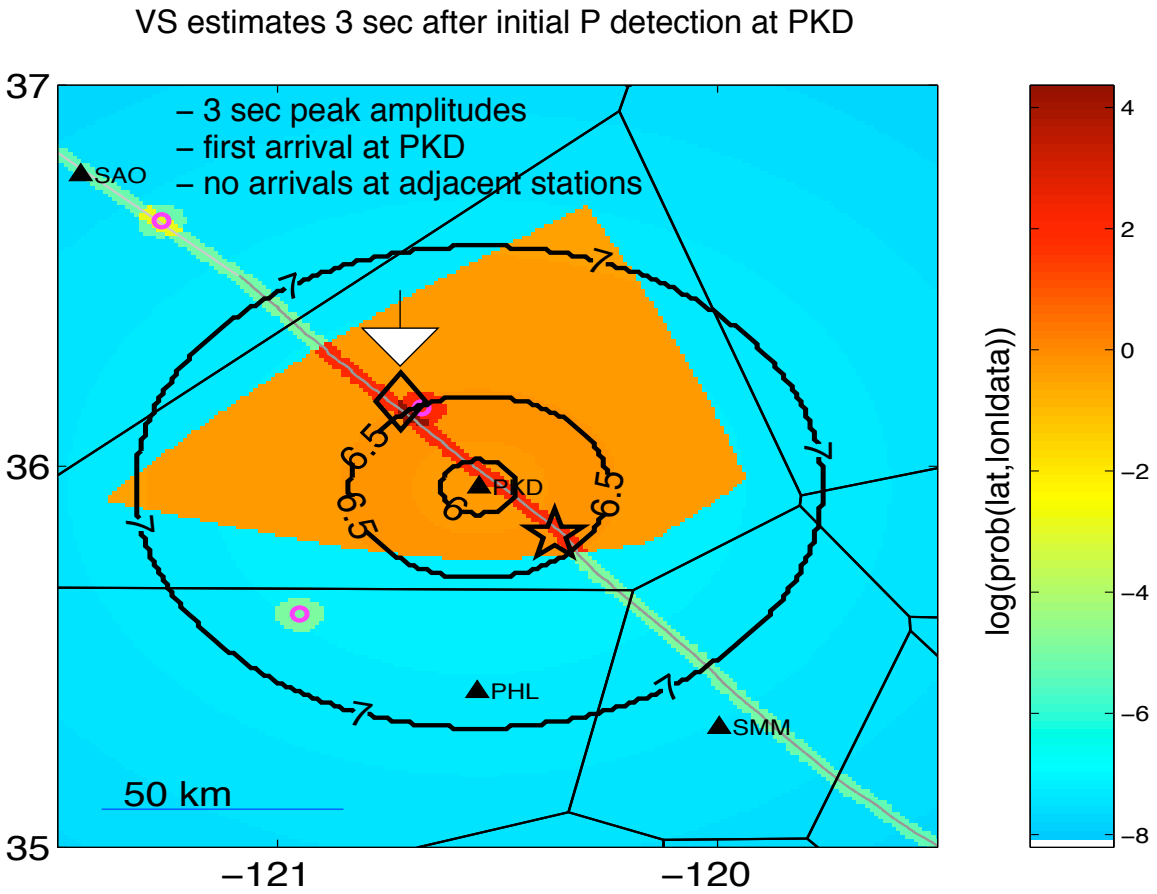

Figure 7.11: The colors correspond to the value of the marginal of the location estimates of the Bayesian posterior pdf, $prob(lat, lon|data)$ (integrating out the effects of magnitude from the posterior pdf $prob(M, lat, lon|data)$). Locations within a 2 km band of the San Andreas *and* within the region consistent with the arrivals (and non-arrivals) in PKD's Voronoi cell have relatively high probability. The best location estimate corresponds to the peak of the location prior (arrow), which is the location of the M1.78 event that occurred the previous day close to the San Andreas. The contours convey the magnitude estimates for the given locations without the Gutenberg-Richter relationship. Without the Gutenberg-Richter (G-R) magnitude-frequency relationship, the magnitude that maximizes the posterior is $M = 6.5 \pm 0.65$, with the G-R, it is $M = 5.5 \pm 0.72$.

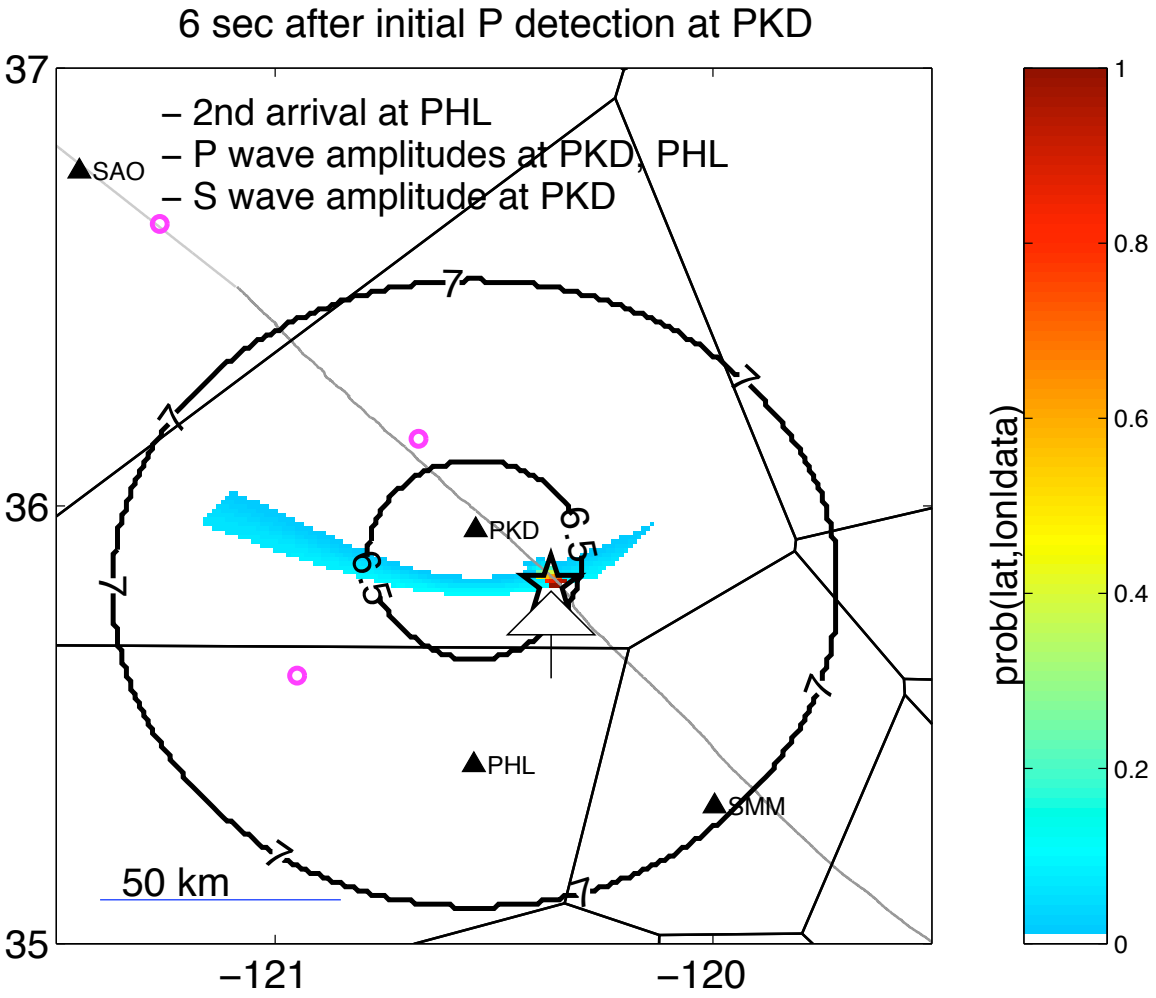

Figure 7.12: The second P arrival is detected at station PHL, approximately 4.4 seconds after the initial P detection at PKD. The epicentral locations consistent with this interval between arrivals lie on a hyperbola defined by $R_{PHL} - R_{PKD} = V \times 4.4$, where V is an average P-wave velocity. The non-arrivals at the other stations limit this hyperbola to the shaded crescent within PKD's Voronoi cell. Without fault information in the Bayes prior, the VS estimates would trade-off along this crescent. With the San Andreas fault trace, the VS location estimate is the intersection of this crescent with the San Andreas. The contours in the Figure show the magnitude estimates without the Gutenberg-Richter relationship. Without the G-R, the magnitude corresponding to the most probable location is $M = 6.4 \pm 0.4$. With the G-R, the corresponding magnitude estimate is $M = 6.1 \pm 0.37$.

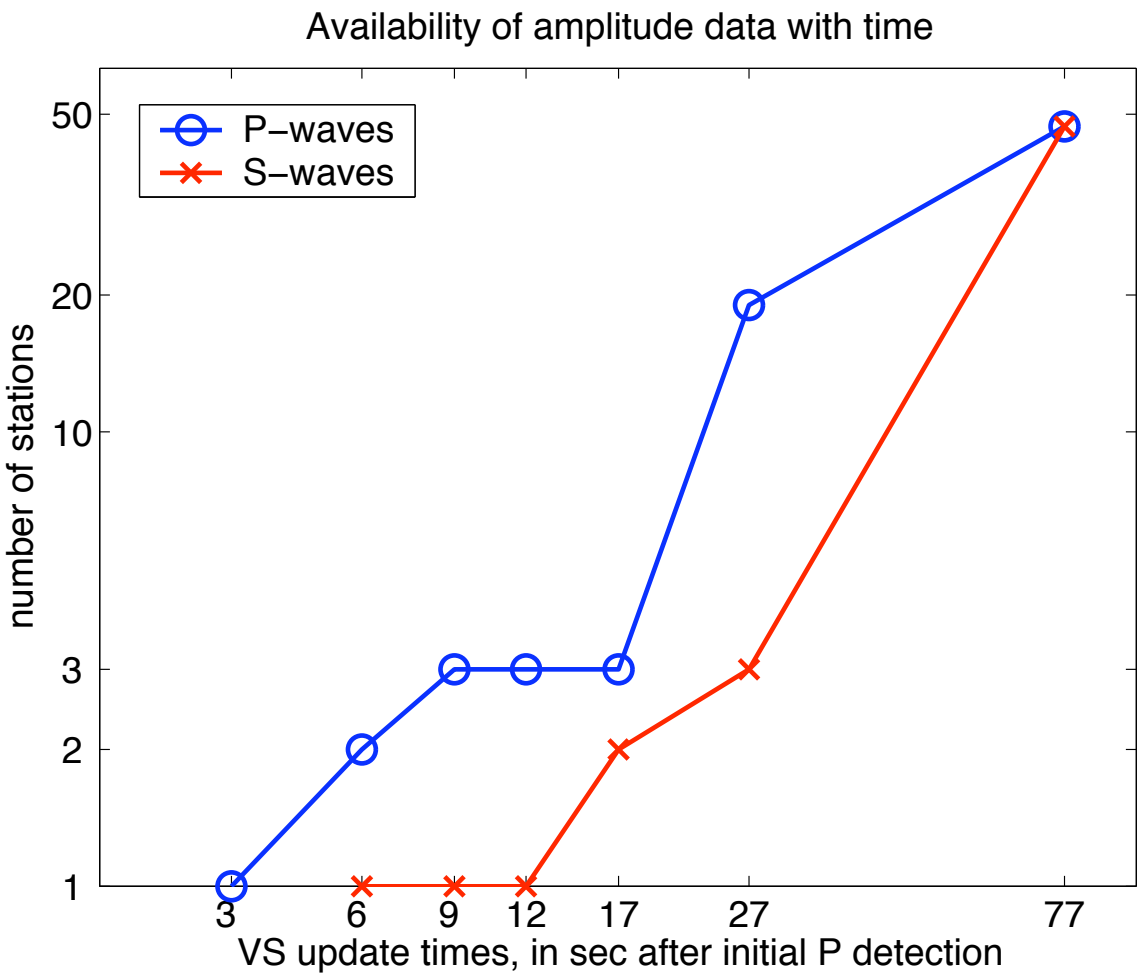

Figure 7.13: The number of stations contributing P- and S-wave amplitudes to the VS estimates as a function of time.

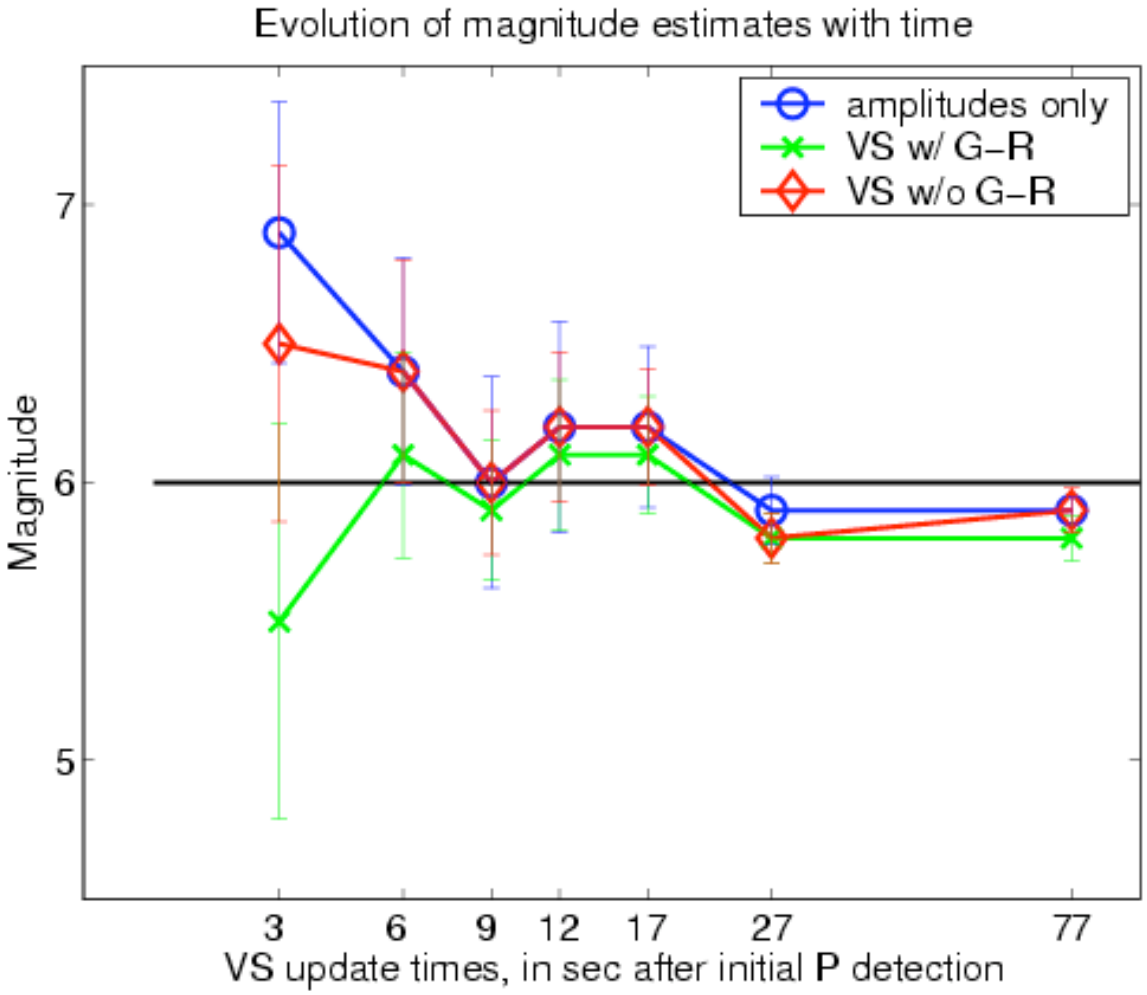

Figure 7.14: The estimates labeled "amplitude only" do not use prior information. The VS magnitude estimates with and without the Gutenberg-Richter relationship in the Bayes prior are shown. The horizontal time marks the SCSN-reported magnitude of M=6.0.

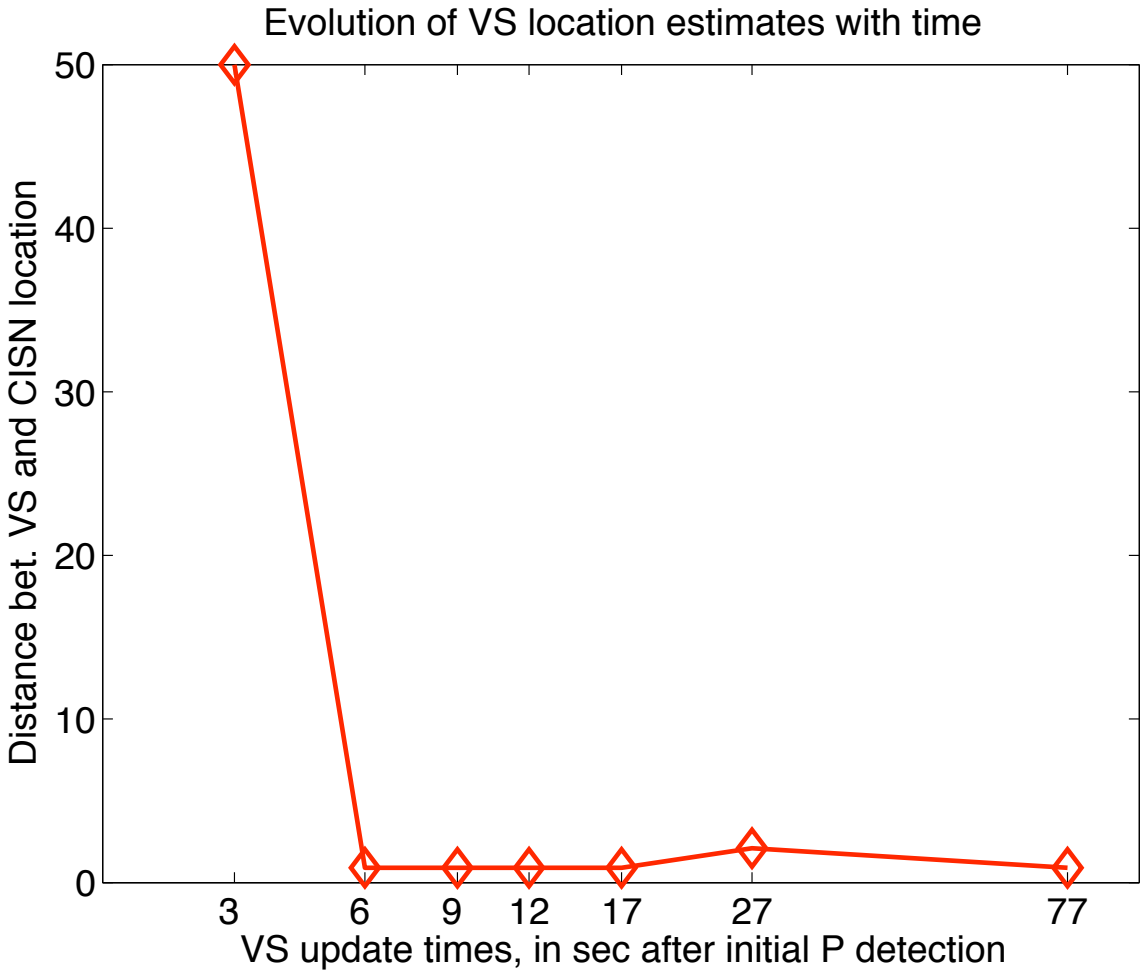

Figure 7.15: The evolution of the VS location estimates as a function of time. The distance between the VS location estimate and the SCSN-reported location is shown. The VS estimates are based on the available amplitudes and arrival information as shown in Figure 7.13.

are very robust (Kanamori, 1993). Figure 7.16 shows contours of the amplitude- and arrival-based location estimates. The arrival-based location estimate was calculated using an average P-wave velocity of 6 km/s. The SCSN-reported location (star) is a much more accurate arrival-based estimate, as it uses a more realistic velocity model. When there is general agreement between the amplitude- and arrival-based location estimates, as in this case, the arrival-based locations are correct.

Figure 7.17 plots the root mean square of the peak observed horizontal S-wave amplitudes (usually equivalent to the peak ground motions) for acceleration, velocity, and filtered displacement as a function of epicentral distance. The solid black lines are the expected ground motion amplitudes for an M=5.9 event using the S-wave envelope attenuation relationships; the dashed lines correspond to $\pm\sigma$ of the expected amplitudes. While the acceleration and velocity amplitudes for PKD fall close to the expected amplitudes for a M=5.9, the displacements are larger than expected. This is perhaps due to PKD being in the forward directivity direction of the rupture. Larger than average displacement would make the magnitude estimate from the ground motion ratio large. Figure 7.18 shows the magnitude estimates from the vertical ground motion ratios alone. PKD, the closest station, has the largest ratio-based magnitude estimate. There does not appear to be a strong distance dependence on the ratio-based magnitude estimates. As with the other events considered, the average (over 47 stations) magnitude estimates from the S-wave vertical amplitude ratio is smaller than that from the P-wave ratios.

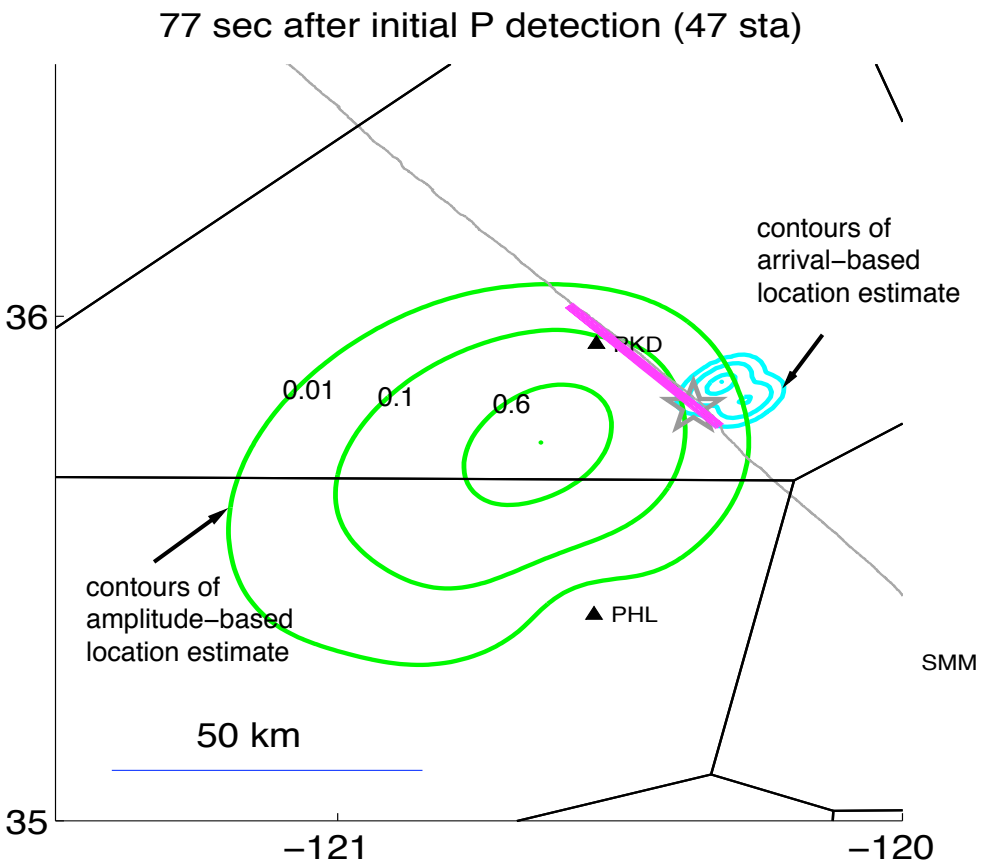

Figure 7.16: Comparison of location estimates based on the spatial distribution of observed amplitudes (green contours) and minimizing the difference between predicted and observed P wave arrival times (blue contours). The amplitude-based estimates(VS estimates using a uniform prior) are less precise but more robust than those based on arrival times; they can be used as a check on the arrival-based estimates, which can be prone to large errors, for example, when there are simultaneous events being recorded by the seismic network. When there is general agreement between these two estimates (as in this situation), the arrival-based locations should be the preferred estimates. For reference, the star shows the location reported by SCSN; the fault trace (in pink) is from a slip inversion by Ji Chen.

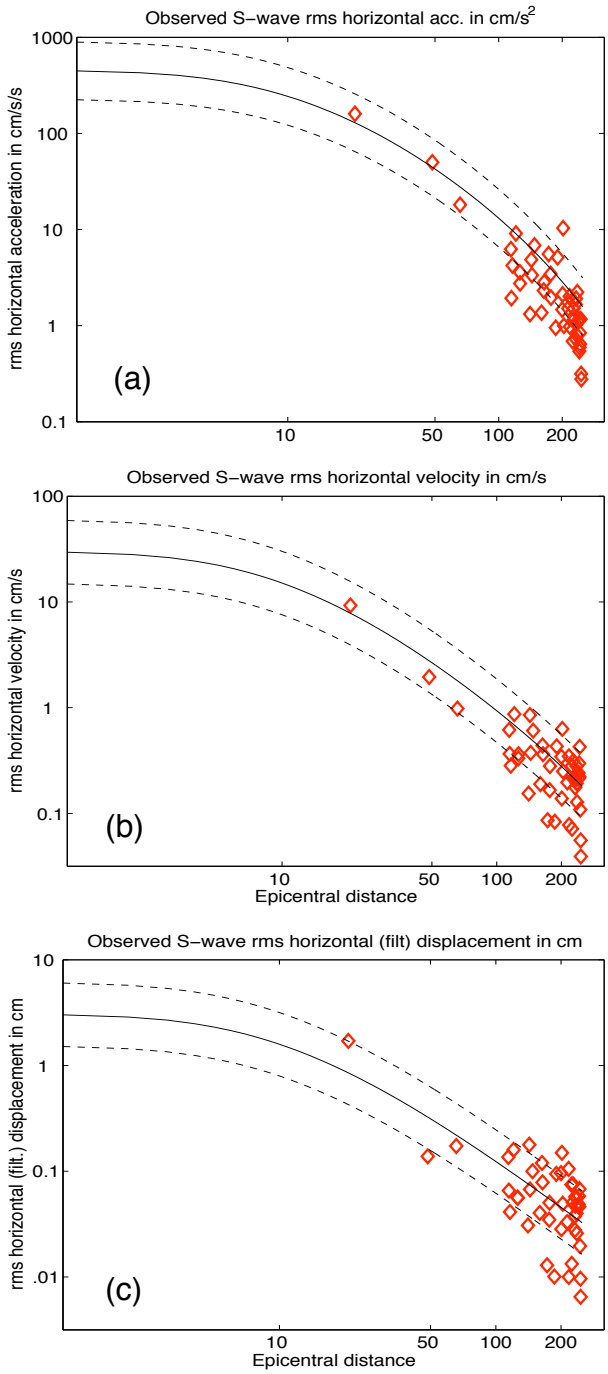

Figure 7.17: Observed peak S-wave rms horizontal amplitudes (usually identical to peak ground motions) plotted against epicentral distance. The envelope attenuation relationships (using M=5.9) are shown in solid black line. The dashed lines are the expected amplitudes $\pm 1\sigma$. Notice that the while the acceleration and velocity amplitudes recorded at PKD (closest station) were close to those expected from the envelope attenuation relationships, the displacement is larger than average. This may explain why initial VS magnitude estimates are large.

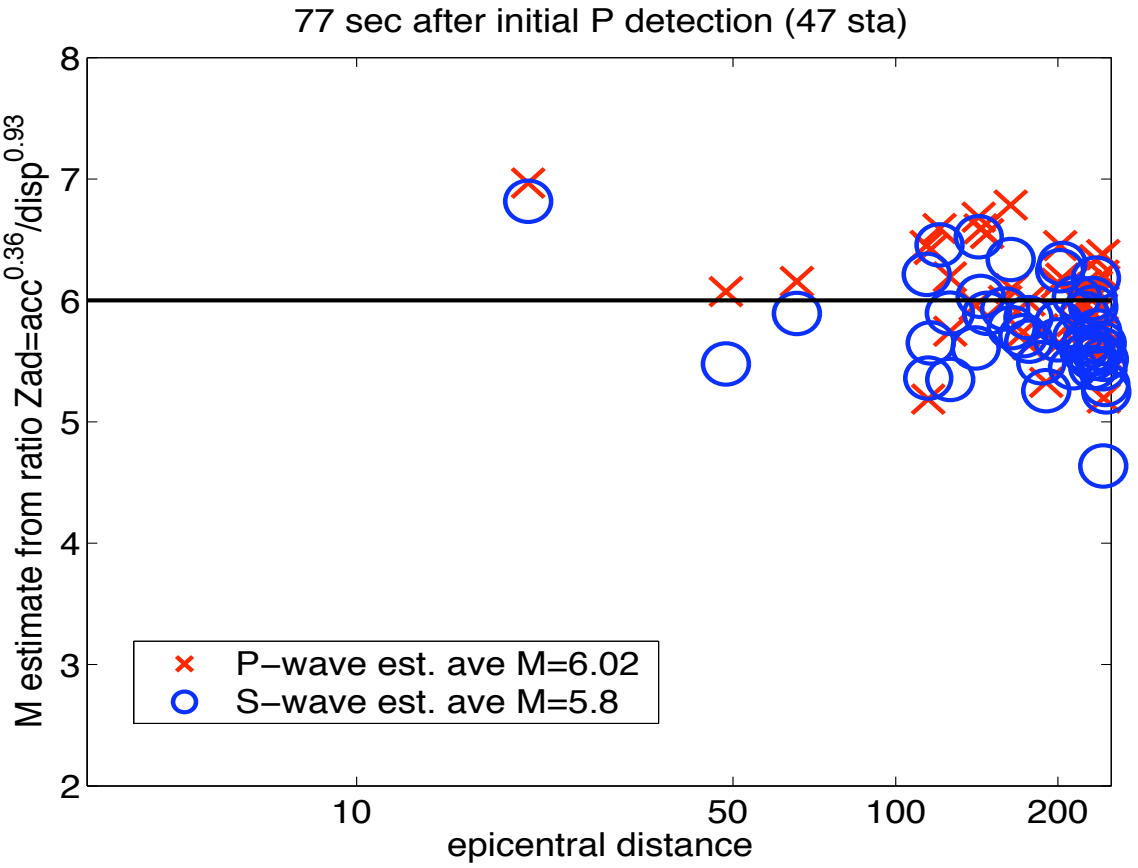

Figure 7.18: The magnitude estimates based on the vertical ground motion ratio $Zad = acc^{0.36}/disp^{0.93}$ for P- and S-waves as a function of distance. If a distance-dependence exists, it is very slight.